STONELEY WAVE PROPAGATION IN A FLUID-FILLED BOREHOLE WITH A VERTICAL FRACTURE

by

X.M. Tang, C.H. Cheng, and M.N. Toksöz

Earth Resources Laboratory
Department of Earth, Atmospheric, and Planetary Sciences
Massachusetts Institute of Technology
Cambridge, MA 02139

ABSTRACT

The propagation of Stoneley waves in a fluid-filled borehole with a vertical fracture is investigated both theoretically and experimentally. The borehole propagation excites fluid motion in the fracture and the resulting fluid flow at the fracture opening perturbs the fluid-solid interface boundary condition at the borehole wall. By developing a boundary condition perturbation technique for the borehole situation, we have studied the effect of this change in the boundary condition on the Stoneley propagation. Cases of both hard and soft formations have been investigated. It has been shown that the fracture has minimal effects on the Stoneley velocity except in the very low frequency range in which the Stoneley velocity drastically decreases with decreasing frequency. Significant Stoneley wave attenuation is produced because of the energy dissipation into the fracture. In general, the effects of the fracture are more important in the low frequency range than at higher frequencies. The quantitative behavior of these effects depends not only on fracture aperture and borehole radius, but also on the acoustic properties of the formation and fluid.

Ultrasonic experiments have been performed to measure Stoneley propagation in laboratory fracture borehole models. Aluminum and lucite were used to simulate a hard and a soft formation, respectively. Array data for wave propagation were obtained and were processed using Prony's method to give velocity and attenuation of Stoneley waves as a function of frequency. In both hard and soft formation cases, the experimental results were found to agree well with the theoretical predictions.

The important result of this study is that, we have found a quantitative relationship between the Stoneley propagation and the fracture character in conjunction with formation and fluid properties. This relationship can be used to provide a method for estimating the characteristics of a vertical fracture by means of Stoneley wave measurements.

INTRODUCTION

An important application of full waveform acoustic logging is the detection of open borehole fractures. Although horizontal and inclined fractures are a common feature encountered in borehole acoustic logging, vertical fractures are of particular interest in certain situations. For example, a fracture resulting from hydraulic fracturing in oil production is often vertical, and its aperture is an important parameter that governs the amount of fluid conducted into (or away from) the borehole. The Stoneley wave has been explored as a means of fracture detection and characterization. In many situations, this wave mode is the most recognizable wave in the full waveform acoustic logs because of its relatively large amplitude and slow velocity. Based on field observations, Paillet and White (1982) have suggested that the Stoneley wave may be the portion of the full waveform which is most indicative of fracture characteristics. If the quantitative relationship between Stoneley propagation and the fracture character can be found, it will provide a method for estimating fracture characteristics by means of Stoneley wave measurements. The objective of this study is to develop a quantitative analysis of Stoneley propagation in the presence of a vertical borehole fracture and to provide the theoretical basis for its application to fracture detection and characterization.

Apart from its practical importance, this problem points to an interesting "leaky" wave-guide phenomenon. Because of a fracture along the borehole wall, the wave propagation is attenuated because of the leakage of wave energy into the fracture. Since the leakage occurs at the fracture opening, it is expected that the problem does not have an axial symmetry and one needs to consider azimuthal distribution of borehole wave motions. Owing to a discontinuity in the formation surrounding the borehole, seeking an exact solution will be a formidable task. We therefore turn to the use of a perturbation theory. We will develop a boundary condition perturbation technique to treat the problem. This technique has been employed to treat acoustic problems involving perturbation of boundary conditions from the ideal "hard" (Neumann) or "soft" (Dirichlet) extremes (Morse and Feshbach, 1953). In the borehole propagation problem, however, the technique needs to be further developed because the boundary condition at the borehole wall is neither ideally hard nor ideally soft, because of the coupling between the borehole fluid and the elastic formation. In addition, because of the non-axial-symmetric nature of the problem, this technique must also take into account the azimuthal borehole fluid motions.

In the following text, we first define the problem of this study. Next we find the elastic motion of the wall as a boundary condition in the absence of the fracture. In the presence of the fracture, we study the fracture fluid motion excited by the borehole propagation and incorporate this effect into the boundary condition. Then the problem is formulated and solved by developing a boundary condition perturbation

technique for the borehole situation. Following the solution of the problem, we present some numerical examples for a hard and a soft formation case. Finally, we describe the laboratory experimental procedure and compare the experimental results with the theoretical predictions.

STATEMENT OF THE PROBLEM

Let us consider a fluid-filled circular cylindrical borehole with a vertical fracture. The fracture is a vertical formation discontinuity having an aperture L, is filled with fluid, and intersects the borehole diametrically (Figure 1). The formation outside the borehole consists of a homogeneous isotropic elastic solid with density ρ, compressional velocity V_p, and shear velocity V_s. The borehole and the fracture are filled with the same fluid with density ρ_f and acoustic velocity V_f. The formation can be either hard ($V_p > V_s > V_f$) or soft ($V_p > V_f > V_s$) with respect to the fluid.

We will use a cylindrical coordinate system (r, θ, z), with z coinciding with borehole axis that is taken to be vertical, r is the radial distance from the center of the borehole, and θ the angle measured from the radial direction that points into the fracture (Figure 1). In the borehole fluid, the fluid displacement potential Ψ satisfies the wave equation

$$\frac{\partial}{\partial r}(r\frac{\partial \Psi}{\partial r}) + \frac{1}{r^2}\frac{\partial^2 \Psi}{\partial \theta^2} + \frac{\partial^2 \Psi}{\partial z^2} + k_0^2 \Psi = 0 \tag{1}$$

where $k_0 = \frac{\omega}{V_f}$ is the acoustic wavenumber of the fluid and ω is the angular frequency. The fluid displacement $\vec{U}$ and pressure P are given by

$$\vec{U} = \nabla \Psi \tag{2}$$

$$P = \rho_f \omega^2 \Psi \tag{3}$$

For a propagation along the positive z direction, Ψ can be written as:

$$\Psi(r, \theta, z) = \psi(r, \theta) exp(ik_z z) \tag{4}$$

where k_z is axial wavenumber. Substitution of Eq. (4) into Eq. (1) results in

$$\nabla_t^2 \psi + \kappa^2 \psi = 0 \tag{5}$$

where

$$\nabla_t^2 = \frac{\partial}{\partial r}(r\frac{\partial}{\partial r}) + \frac{1}{r^2}\frac{\partial^2}{\partial \theta^2} \tag{6}$$

is the two-dimensional Laplace operator, and $\kappa = \sqrt{k_0^2 - k_z^2}$ is the radial wavenumber. Eq. (5) will be solved in conjunction with the boundary condition at the borehole wall.

In the absence of a vertical discontinuity in the elastic formation, solutions have long been available for wave motions both in the formation solid and in the borehole fluid (Biot, 1952; Cheng and Toksöz, 1981). The two solutions are matched at the borehole wall using continuity conditions. Consequently, the elastic motion of the wall is specified. We may treat the known wall motion as a boundary condition prescribed at the borehole boundary. In the presence of the vertical fracture, this boundary condition will be perturbed. To know the extent to which the boundary condition is changed, we need to study the fluid motion in the fracture and its interaction with the borehole fluid motion. The effect of this change in the boundary condition on the borehole Stoneley propagation will be investigated by means of the boundary condition perturbation technique.

BOUNDARY CONDITION WITHOUT FRACTURE

For a fluid-filled borehole of radius R in an unfractured elastic formation, we now prescribe the elastic motion at the wall as a boundary condition for the borehole fluid motion. According to Eqs. (2), (3), and (4), we may relate the potential $\psi(r,\theta)$ and its radial derivative through the following equation

$$\frac{\partial \psi}{\partial r} - (\rho_f \omega^2 \frac{U}{P})\psi = 0 \quad . \tag{7}$$

where U is the radial fluid displacement. At the radial boundary $r = R$, we have the continuity of radial stress and displacement. These conditions can be expressed through a match of the wall impedance (Biot, 1952)

$$\frac{P}{U} = -\frac{\sigma}{U_w} \tag{8}$$

where σ and U_w are the elastic radial stress and displacement at the borehole wall, respectively. Eq. (8), together with the condition that the elastic shear stresses vanish at the wall, leads to a dispersion equation given by (Cheng et al., 1982)

$$\frac{I_0(fR)}{fI_1(fR)} = \frac{\rho}{\rho_f l}\left\{\frac{2V_s^2 lg}{k_z^2 c^2}\left[\frac{1}{gR} + \frac{2V_s^2}{c^2}\frac{K_0(gR)}{K_1(gR)}\right] - (\frac{2V_s^2}{c^2} - 1)^2 \frac{K_0(lR)}{K_1(lR)}\right\} \tag{9}$$

with the radial wavenumbers l, g, and f given as

$$l = k_z\sqrt{1 - \frac{c^2}{V_p^2}} \quad , \quad g = k_z\sqrt{1 - \frac{c^2}{V_s^2}} \quad , \quad f = k_z\sqrt{1 - \frac{c^2}{V_f^2}} \quad . \tag{10}$$

where I_0, I_1, K_0, and K_1 are modified Bessel functions of the first and second kind of order zero and one, respectively. V_p, V_s, V_f, ρ, ρ_f, and R have all been defined

previously. c is the phase velocity of wave modes. Eq. (9) has an infinite number of solutions for c, giving rise to different wave modes. Specifically, for a hard formation, an infinite number of pseudo-Rayleigh (or normal) modes exist (Biot, 1952; Cheng and Toksöz, 1981), while for a soft formation, an infinite number of leaky-P modes exist (Paillet and Cheng, 1986). In both situations, a fundamental mode – Stoneley mode exists for all frequencies. Depending on whether the mode velocity c is greater or smaller than the fluid acoustic velocity V_f, Eq.(7), evaluated at $r = R$, can be written as

$$\frac{\partial \psi}{\partial r} - \left[\frac{fI_1(fR)}{I_0(fR)}\right]\psi = 0 \quad (c < V_f, \quad \text{Stoneley mode}) \tag{11}$$

$$\frac{\partial \psi}{\partial r} + \left[\frac{fJ_1(fR)}{J_0(fR)}\right]\psi = 0 \quad (c > V_f, \quad \text{other modes}) \tag{12}$$

where J_0 and J_1 are Bessel functions of the first kind of order zero and one, respectively. It is noted that Eq. (11) or (12) has the form of the conventional mixed (or the third) boundary condition. A somewhat "unconventional" point in this boundary condition is that the coefficient in front of ψ assumes different values depending on different wave modes determined by Eq. (9). However, as we will see later, since our perturbation theory applies to one particular wave mode (e.g., Stoneley mode in the present study), we can still treat Eq. (11) or (12) as the conventional mixed boundary condition for this particular wave mode.

BOUNDARY CONDITION WITH FRACTURE

In the presence of the vertical fracture, the boundary condition at the borehole wall will be perturbed. We assume that significant change in the boundary condition occurs mainly at the fracture opening, so that the boundary condition (for the Stoneley) away from the fracture can still be approximated by Eq. (11). This assumption is based on the laboratory experimental observation (which we will show later) that the Stoneley velocity along a fractured borehole does not differ significantly from that along an unfractured borehole. This indicates that the boundary condition as a whole is not significantly changed and the change should be mainly at the fracture opening. Therefore, for the solid part of the borehole wall we have

$$\frac{\partial \psi}{\partial r} - h_0\psi = 0 \quad (\text{solid part of the wall}) \quad , \tag{13}$$

where $h_0 = \dfrac{fI_1(fR)}{I_0(fR)}$. Whereas for the fluid part of the wall where the fracture opening is located, the boundary condition will be determined by the interaction between the borehole and the fracture fluid systems. When a borehole acoustic wave propagates along the fracture opening, wave motion will be excited in the fracture, which in

turn will affect the borehole propagation. For this reason, we need to know how much motion is excited. By extending Darcy's law into the dynamic regime, Tang and Cheng (1988) have given a quantitative measure for the amount of fluid flow conducted into a fracture at its opening

$$Q = -\bar{C}\frac{\partial P}{\partial y} \tag{14}$$

where Q is the volume flow rate per unit fracture length, $\frac{\partial P}{\partial y}$ is the dynamic pressure gradient normal to the fracture opening. $\bar{C}$ is the dynamic conductivity governed by both effects of viscous shear at the fracture surface and wave propagation along the fracture. It has been shown (Tang and Cheng, 1988) that, when the viscous skin depth $\delta = \sqrt{\frac{2\nu}{\omega}}$ (ν = kinematic viscousity) is small compared to the fracture aperture L, $\bar{C}$ is given by a simple formula

$$\bar{C} = \frac{iL}{\omega\rho_f} \quad (L \gg \delta) \quad . \tag{15}$$

At logging frequencies of a few kilohertz, δ is the order of 10 to 100 μm, depending on viscosity. The fracture aperture we are dealing with is the order of millimeter to centimeter. Thus the use of Eq. (15) is well justified. We will neglect viscous effects in this study. The determination of the pressure gradient in Eq. (14) needs the knowledge of fluid motion in the fracture.

Fracture Wave Excited by Borehole Propagation

Consider the Cartesian coordinate system (x, y, z) shown in Figure 1, where the fracture surfaces are located at $x = -L/2$ and $x = L/2$, z is parallel with the borehole axis, and y is measured from the fracture opening and is pointed into the fracture. The fracture fluid pressure P_f satisfies the scalar wave equation

$$\nabla^2 P_f + k_0^2 P_f = 0 \quad , \tag{16}$$

where $\nabla^2 = \frac{\partial^2}{\partial x^2} + \frac{\partial^2}{\partial y^2} + \frac{\partial^2}{\partial z^2}$. In terms of P_f, the fluid displacement is given by

$$\vec{U}_f = \frac{\nabla P_f}{\rho_f \omega^2} \tag{17}$$

In the elastic solid bonding the fracture, a general solution to the vector equation of motion can be written as (Pilant, 1979)

$$\vec{u} = \nabla\Phi - \nabla \times \nabla \times (\vec{e}_x\Omega) + \nabla \times (\vec{e}_x\Lambda) \quad , \tag{18}$$

where $\vec{u}$ is the elastic displacement, $\vec{e}_x$ is the unit vector along x axis, and Φ, Ω, and Λ satisfy the following wave equations:

$$\begin{aligned} \nabla^2\Phi + \frac{\omega^2}{V_p^2}\Phi &= 0 \quad , \\ \nabla^2\Omega + \frac{\omega^2}{V_s^2}\Omega &= 0 \quad , \\ \nabla^2\Lambda + \frac{\omega^2}{V_s^2}\Lambda &= 0 \quad . \end{aligned} \tag{19}$$

They represent P-wave, SV-wave, and SH-wave motions, respectively. The elastic stresses σ_{ij} are given by the constitutive relation for an isotropic elastic solid:

$$\sigma_{ij} = \lambda(\frac{\partial u_k}{\partial x_k})\delta_{ij} + \mu(\frac{\partial u_i}{\partial x_j} + \frac{\partial u_j}{\partial x_i}) \quad , \tag{20}$$

where δ_{ij} is the Krokener delta and λ and μ are elastic moduli. $x_1 = x$, $x_2 = y$, and $x_3 = z$. σ_{ij} $(i, j = 1, 2, 3)$ represents the stress system $(\sigma_{xx}, \sigma_{yy}, \sigma_{zz}, \sigma_{xy}, \sigma_{xz}, \sigma_{yz})$. Because of a propagating borehole pressure wave $P(\omega)exp(ik_z z)$ along the fracture opening, the propagation in the fracture has two components. The first is the propagation along z direction to comply with the borehole propagation, given by $exp(ik_z z)$. The second is the propagation towards y direction, denoted by $exp(ik_y y)$. The latter propagation is initiated by the pressure difference between the borehole and the fracture fluid. Taking this two-dimensional propagation into account and considering the fact that the borehole pressure $P(\omega)$ is symmetric with respect to x, we have solutions to Eqs. (16) and (19) in the form of

$$\begin{bmatrix} P_f \\ \Phi \\ \Omega \\ \Lambda \end{bmatrix} = \begin{bmatrix} P_{f0} cosqx \\ \Phi_0 e^{-q_p|x|} \\ \Omega_0 e^{-q_s|x|} \\ \Lambda_0 e^{-q_s|x|} \end{bmatrix} exp(ik_y y)exp(ik_z z) \quad , \tag{21}$$

where

$$q = \sqrt{\frac{\omega^2}{V_f^2} - k_y^2 - k_z^2}, \quad q_p = \sqrt{k_y^2 + k_z^2 - \frac{\omega^2}{V_p^2}}, \quad q_s = \sqrt{k_y^2 + k_z^2 - \frac{\omega^2}{V_s^2}}.$$

Substitution of the solutions in Eqs. (21) into Eqs. (17), (18), and (20) yields fluid displacement in fracture and elastic stresses and displacement in solid. The boundary conditions at solid-fluid interfaces $x = \pm L/2$ are the vanishing of shear stresses

$$\begin{aligned} \sigma_{xy} &= 0 \\ \sigma_{xz} &= 0 \end{aligned} \tag{22}$$

and the continuity of normal stress and displacement. This continuity condition can be expressed by an impedance equation (Ferrazzini and Aki, 1987)

$$\frac{P_f}{U_f} = -\frac{\sigma_{xx}}{u_x} \quad (x = \pm\frac{L}{2}) \tag{23}$$

Eqs. (22) result in the vanishing of SH-wave motion in the elastic solid (i.e., $\Lambda_0 = 0$). This is to be expected since the type of coupling between solid and fluid as stated in Eqs. (22) and (23) only allows P-SV waves to exist. Eqs. (22) and (23) lead to the following dispersion equation:

$$cot\left(\frac{L\omega}{2v}\sqrt{\frac{v^2}{V_f^2}-1}\right) = \frac{\rho V_s^4\sqrt{\frac{v^2}{V_f^2}-1}}{\rho_f v^4\sqrt{1-\frac{v^2}{V_p^2}}}\left[\left(2-\frac{v^2}{V_s^2}\right)^2 - 4\sqrt{1-\frac{v^2}{V_s^2}}\sqrt{1-\frac{v^2}{V_p^2}}\right] \quad , \tag{24}$$

where v is the phase velocity of the wave modes existing in the fracture and *cot* represents the cotangent function. The same dispersion equation has been obtained by several authors (Ferrazzini and Aki, 1987; Paillet and White, 1982) for one-dimensional propagation cases. Here we rederived it for the general two-dimensional propagation case. It should be understood that the fracture wavenumber k determined by Eq. (24) is related to k_y and k_z via

$$k = \frac{w}{v} = \sqrt{k_y^2 + k_z^2} \tag{25}$$

The wave modes determined by the dispersion equation (Eq. 24) have been experimentally confirmed by a laboratory measurement (Tang and Cheng, 1988). Analogous to the dispersion equation (Eq. 9) for the borehole modes, Eq. (24) results in an infinite number of normal or leaky-P wave modes, depending on whether the solid is hard or soft with respect to the fracture fluid. In particular, a fundamental mode analogous to the borehole Stoneley mode exists for all frequencies. However, the velocity of this fundamental mode goes to zero at very low frequencies (see Tang and Cheng, 1988) while the velocity of the borehole Stoneley mode approaches a finite value. Although a number of wave modes may exist in the fracture, the fundamental mode is the most important one that interests us. We assume that the borehole pressure is nearly uniform over the fracture aperture, since the aperture is generally small compared to the borehole perimeter. If the formation is rigid, the uniform pressure at the opening excites only the fundamental mode in the fracture. It is reasonable to assume that the borehole pressure will mostly excite the fundamental fracture wave mode when the formation is elastic. We have verified this assumption by numerically evaluating the amplitude of each mode excited by a uniform pressure at the opening. We found that the fundamental mode indeed dominates even in the case of a soft elastic formation. We will therefore only consider the interaction of the fundamental fracture wave mode with the borehole propagation. When the fundamental mode velocity is found

by solving Eq. (24), the fracture fluid wavenumber is given by

$$k_{fr} = \frac{\omega}{v} \quad . \tag{26}$$

By averaging the fracture pressure in Eqs. (21) over the fracture aperture L and matching it with the borehole pressure $P(\omega, R)$ at the fracture opening, it is readily shown that the pressure gradient in Eq. (14) (averaged over the fracture aperture) is given by

$$\frac{\partial P}{\partial y} = ik_y P(\omega, R) \tag{27}$$

where

$$k_y = \sqrt{k_{fr}^2 - k_z^2} \quad . \tag{28}$$

A few remarks will help to illustrate the interaction between the fundamental fracture wave and the borehole propagation. The wave front in the fracture has an angle $\alpha = sin^{-1}(\frac{k_y}{k_{fr}})$ with respect to the wave front in the borehole. As we have mentioned before, at very low frequencies, the fracture wave velocity goes to zero, while the (unfractured) borehole Stoneley velocity approaches a finite value. Thus $k_{fr} \gg k_z$ and $\alpha \rightarrow \frac{\pi}{2}$. The borehole pressure pushes the fluid radially into the fracture, causing strong interaction between the two fluid systems. Whereas at high frequencies, both the fracture and the borehole velocities approach the Stoneley velocity along the fluid-solid interface (i.e., Scholte velocity). Thus $k_y \sim 0$ and $\alpha \rightarrow 0$; the fracture wave motion is nearly in phase with the borehole propagation, resulting in minimal interaction. It is therefore expected that the effects of the fracture will be more significant at low frequencies than at higher frequencies.

Boundary Condition for Entire Wall

With $\bar{C}$ and $\frac{\partial P}{\partial y}$ known, Eq. (14) can be used to determine the average radial fluid displacement $\overline{U}$ at the fracture opening. Since Q, the unit-length flow rate, is the integral of flow velocity (given by $-i\omega U$) over the aperture L, the average displacement is given by

$$\overline{U} = \frac{Q}{-i\omega L} = \frac{ik_y}{\rho_f \omega^2} P(\omega, R) \quad . \tag{29}$$

By using Eq. (7), Eq. (29) can be expressed in terms of the displacement potential ψ.

$$\frac{\partial \psi}{\partial r} - ik_y \psi = 0 \ , \quad \text{(at fracture opening)} \ . \tag{30}$$

Combining Eqs. (13) and (30), we can write the boundary condition for the entire borehole wall as

$$\frac{\partial \psi}{\partial r} - h_0 \psi + (-ik_y + h_0) W(\theta) \psi = 0 \ , \quad (\text{at } r = R) \quad , \tag{31}$$

where

$$W(\theta) = \begin{cases} 1 & -\frac{L}{2R} \le \theta \le \frac{L}{2R} \\ 1 & \pi - \frac{L}{2R} \le \theta \le \pi + \frac{L}{2R} \\ 0 & \text{otherwise} \end{cases}$$

Because the coefficient in front of ψ is the function of the azimuthal variable θ in this boundary condition, Eq. (5) cannot be solved using the conventional method of separation of variables. We therefore have to seek approximate solutions using the perturbation theory.

FORMULATION OF BOUNDARY CONDITION PERTURBATION

For a perturbation theory, we may treat $(-ik_y + h_0)W(\theta)$ in Eq. (31) as a perturbation to the original boundary condition $\frac{\partial \psi}{\partial r} - h_0\psi = 0$. Although the term $(-ik_y + h_0)$ may not be a small quantity at the fracture opening, the fracture aperture is generally small compared to the borehole perimeter, such that its overall effect on the borehole propagation is a perturbation. It is therefore convenient to consider the solutions to the unperturbed boundary value problem as basis functions

$$\begin{cases} \nabla_t^2 \phi_{mn} + \kappa_{mn}^2 \phi_{mn} = 0 \\ \frac{\partial \phi_{mn}}{\partial r} - h_0 \phi_{mn} = 0 \qquad (\text{at } r = R) \end{cases} \tag{32}$$

where κ_{mn}'s are the eigenvalues of the problem and ϕ_{mn} are the associated eigen functions that form a complete orthogonal set. Using the conventional method of separation of variables, solutions of Eq. (32) are readily found, as given by

$$\phi_{mn} = \frac{1}{\sqrt{\pi N_{mn} \epsilon_m}} \begin{Bmatrix} cosm\theta \\ sinm\theta \end{Bmatrix} J_m(\gamma_{mn} \frac{r}{R}) \quad , \tag{33}$$

with

$$\begin{cases} m = & 0, 1, 2, \cdots \\ n = & 1, 2, 3, \cdots \end{cases} \quad \text{and} \quad \epsilon_m = \begin{cases} 2 & m = 0 \\ 1 & m > 0 \end{cases} \quad ,$$

where

$$N_{mn} = \frac{R^2}{2} \left\{ [J_m'(\gamma_{mn})]^2 + (1 - \frac{m^2}{\gamma_{mn}^2})[J_m(\gamma_{mn})]^2 \right\} \tag{34}$$

is the normalization factor, J_m is the mth order Bessel function of the first kind, and

$$\gamma_{mn} = \kappa_{mn} R$$

is the nth root of the following equation:

$$\gamma \frac{dJ_m(\gamma)}{d\gamma} - h_0 R J_m(\gamma) = 0 \tag{35}$$

This equation is derived from the boundary condition of Eq. (32). Eq. (35) gives a set of eigenvalues κ_{mn} and determines their associated eigen functions ϕ_{mn} (Eq. 33). Note that $h_0 R$ in this equation has to be found by solving the borehole dispersion equation for the Stoneley mode. Consequently, the set $\{\phi_{mn}\}$ can be regarded as the sub-set (or sub-modes) of the Stoneley mode. (Analogously, there are sub-modes for the pseudo-Rayleigh modes and leaky-P modes.) The non-dimensional quantity $h_0 R = \frac{fRI_1(fR)}{I_0(fR)}$ depends on the formation and fluid properties. In fact, it characterizes the compliance of the borehole wall with respect to the borehole fluid. Figure 2 shows $h_0 R$ as the function of frequency for both hard and soft formations surrounding a fluid-filled borehole of a given radius. As shown in this figure, $h_0 R$ is small for a hard formation and large for a soft formation. In the extremely hard formation case, $h_0 R$ approaches zero and Eq. (35) corresponds to the rigid boundary condition. For this case, the roots of $J'_m(\gamma) = 0$ are available (Abramowitz and Stegun, 1970). For an elastic formation of finite rigidity, $h_0 R$ has a finite value and the roots of Eq. (35) have to be determined for the different values of $h_0 R$. What makes Eq. (11) or (35) special is the negative sign in front of the coefficient of ψ or of $J_m(\gamma)$. In this place, the commonly encountered third boundary condition has a positive sign. Doak and Vaidya (1970) have studied the behavior of the roots of the Eq. (35) type equation. Based on their results, we draw the following two useful properties.

- For $n = 1$, γ_{m1} is imaginary if $h_0 R > m$ and is real if $h_0 R \leq m$.
- For $n > 1$, all γ_{mn}'s are real regardless whether $h_0 R > m$ or $h_0 R \leq m$. They are interplaced with the roots of $J'_m(\gamma) = 0$.

Thus if γ_{mn}'s are real, they can be found by solving Eq. (35) using the roots of $J'_m(\gamma) = 0$ as an initial guess. While when $\gamma_{m1} = i\bar{\gamma}_m$ is imaginary, $\bar{\gamma}_m$ can be found as the single root of

$$\bar{\gamma} \frac{dI_m(\bar{\gamma})}{d\bar{\gamma}} - h_0 R I_m(\bar{\gamma}) = 0 \quad , \tag{36}$$

where I_m is the mth order modified Bessel function, resulting from the imaginary argument of J_m. The fact that γ_{mn} has imaginary solutions indicates the presence of the Stoneley type modes in the sub-set $\{\phi_{mn}\}$ (the Stoneley has a radial function of I instead of J). In this case, $\{\phi_{mn}\}$ still forms a complete, orthogonal real set (Watson,

1941). With a slight modification, this set can be written as:

$$\begin{cases} \phi_{m1} = \sqrt{\dfrac{2}{\pi R^2 \epsilon_m}} \dfrac{\bar{\gamma}_m}{\sqrt{\bar{\gamma}_m^2 - (h_0 R)^2 + m^2}} \left\{ \begin{array}{c} cosm\theta \\ sinm\theta \end{array} \right\} \dfrac{I_m(\bar{\gamma}_m \frac{r}{R})}{I_m(\bar{\gamma}_m)} & (\gamma_{m1} = \text{imaginary}) \\ \phi_{mn} = \sqrt{\dfrac{2}{\pi R^2 \epsilon_m}} \dfrac{\gamma_{mn}}{\sqrt{\gamma_{mn}^2 + (h_0 R)^2 - m^2}} \left\{ \begin{array}{c} cosm\theta \\ sinm\theta \end{array} \right\} \dfrac{J_m(\gamma_{mn} \frac{r}{R})}{J_m(\gamma_{mn})} & (\gamma_{mn} = \text{real}) \end{cases} \tag{37}$$

where we have used Eq. (35) in the normalization factor N_{mn} given by Eq. (34). Having obtained the unperturbed eigen functions ϕ_{mn}, we now use them to formulate the boundary condition perturbation theory. To develop, we employ the two-dimensional Green's function $G(\vec{r}, \vec{r}_0; \omega)$ satisfying the same mixed boundary condition as Eq. (32) at the borehole boundary $r = R$.

$$\begin{cases} \nabla_t^2 G + \kappa^2 G = -4\pi\delta(\vec{r} - \vec{r}_0) \\ \dfrac{\partial G}{\partial r} - h_0 G = 0 \qquad (\text{at } r = R) \end{cases} \tag{38}$$

where ∇_t^2 has been defined in Eq. (6), $\delta(\vec{r} - \vec{r}_0)$ represents the two-dimensional Dirac function, and the two-dimensional vectors

$$\vec{r}_0 = \left\{ \begin{array}{c} r_0 cos\theta_0 \\ r_0 sin\theta_0 \end{array} \right\} \quad \text{and} \quad \vec{r} = \left\{ \begin{array}{c} r cos\theta \\ r sin\theta \end{array} \right\}$$

are the source and field positions, respectively. Using the eigen functions $\{\phi_{mn}\}$, we expand the Green's function with waiting-to-be-determined coefficients and the Dirac function with known coefficients. Substituting the expansions into Eq. (38) and comparing the coefficients on both sides of the equation, we obtain the series solution for the Green's function:

$$\begin{aligned} G(\vec{r}, \vec{r}_0; \omega) &= 4\pi \sum_{m,n} \frac{cos[m(\theta - \theta_0)]}{(\kappa_{mn}^2 - \kappa^2) N_{mn}} J_m(\gamma_{mn} \frac{r_0}{R}) J_m(\gamma_{mn} \frac{r}{R}) \\ &= 4\pi \sum_{m,n} \frac{\phi_{mn}(\vec{r}) \phi_{mn}(\vec{r_0})}{\kappa_{mn}^2 - \kappa^2} \end{aligned} \tag{39}$$

Applying the two-dimensional Green's theorem

$$\int\int_A [G \nabla_t^2 \psi - \psi \nabla_t^2 G] dA = \oint_S [G \frac{\partial \psi}{\partial r} - \psi \frac{\partial G}{\partial r}] dS \quad , \tag{40}$$

where

$$A : \text{borehole area}; \quad S : \text{borehole boundary } r_0 = R$$

to Eqs. (5) and (38), we get

$$4\pi\psi(\vec{r}, \omega) = \oint_S [G \frac{\partial \psi}{\partial r} - \psi \frac{\partial G}{\partial r}] dS \tag{41}$$

Note that the integrand in Eq. (41) is evaluated with the source point on the borehole boundary $r_0 = R$. Thus the boundary conditions for ψ and G (Eqs. 31 and 38) can be used. Substituting $\frac{\partial G}{\partial r} = h_0 G$ and $\frac{\partial \psi}{\partial r} = h_0\psi - (-ik_y + h_0)W(\theta)\psi$ into Eq. (41) and letting $\vec{r}$ approach $\vec{r}_0$ on the boundary, we obtain the following integral equation for $\psi(\vec{r}_0)$:

$$\psi(\vec{r}_0,\omega) = -\frac{1}{4\pi}\oint_S h(S)G(\vec{r}_0,\vec{r}_0;\omega)\psi(\vec{r}_0,\omega)dS \tag{42}$$

with

$$h(S) = (-ik_y + h_0)W(\theta) \ , \ (S = R\theta) \ . \tag{43}$$

Eq. (42) is a second kind homogeneous Fredholm integral equation and can be solved by successive approximations. We assume that $\psi(\vec{r}_0,\omega)$, being the perturbed wave function, can be expanded using the unperturbed eigen functions (or sub-modes)

$$\psi(\vec{r}_0,\omega) = \sum_{m,n} C_{mn}\phi_{mn}(\vec{r}_0,\omega) \tag{44}$$

where C_{mn}'s are the expansion coefficients. In the unfractured borehole case, the Stoneley mode itself suffices to satisfy the axial-symmetric boundary condition (Eq. 11), whereas in the fractured borehole case, the Stoneley sub-modes combine to form a wave packet, in order to satisfy the azimuthally varying boundary condition (Eq. 31). Substitution of Eqs. (39) and (44) into Eq. (42) results in

$$\sum_{m,n} C_{mn}\phi_{mn} = \sum_{m,n}\left(\frac{\sum_{p,q} C_{pq}h_{mnpq}}{\kappa^2 - \kappa_{mn}^2}\right)\phi_{mn} \ , \tag{45}$$

where

$$h_{mnpq} = \oint_S h(S)\phi_{mn}(\vec{r}_0)\phi_{pq}(\vec{r}_0)dS \ .$$

An analysis of the fracture and borehole geometry shown in Figure 1 indicates that the fluid motion in the borehole is symmetric with respect to the diameters coinciding with $\theta = 0$ and $\theta = \frac{\pi}{2}$, so that the azimuthal function of ϕ_{mn} (Eq. 33 or 37) has only $cosm\theta$ component, and the integer m must be even numbers. Using this fact and the $h(S)$ given in Eq. (43), we can readily integrate h_{mnpq} out as

$$\begin{aligned} h_{mnpq} &= \frac{4(-ik_y + h_0)}{\pi R\sqrt{\epsilon_m\epsilon_p}}\frac{\gamma_{mn}\gamma_{pq}}{\sqrt{[\gamma_{mn}^2 + (h_0R)^2 - m^2][\gamma_{pq}^2 + (h_0R)^2 - p^2]}} \\ &\times \begin{cases} \dfrac{sin[(m-p)\frac{L}{2R}]}{m-p} + \dfrac{sin[(m+p)\frac{L}{2R}]}{m+p} & , \quad m \neq p \\ \dfrac{L}{2R} + \dfrac{1}{2m}sin(\dfrac{mL}{R}) & , \quad m = p \neq 0 \\ \dfrac{L}{R} & , \quad m = p = 0 \end{cases} \end{aligned} \tag{46}$$

with

$$\begin{cases} m,p = & 0,2,4,\cdots \\ n,q = & 1,2,3,\cdots \end{cases},$$

where γ_{mn} and γ_{pq} can be real or imaginary depending on the solution to Eq. (35). From Eq. (45), we obtain a set of linear simultaneous equations for the coefficients C_{mn}.

$$\sum_{p,q}[(\kappa^2 - \kappa_{mn}^2)\delta_{mp}\delta_{nq} - h_{mnpq}]C_{pq} = 0 \tag{47}$$

The matrix of this equation is of infinite dimension because m, n, p, and q can go to infinity. In practice, however, this problem can be approximately solved by making the matrix finite dimensional (Bender and Orzag, 1978). We truncate the series in Eq. (45) at $m = M$ (M is an even number) and $n = N$. Eq. (47) may thus be written as

$$\mathbf{HC} = \mathbf{0} \quad , \tag{48}$$

where $\mathbf{H}$ is a $(\frac{M}{2}+1)N \times (\frac{M}{2}+1)N$ symmetric square matrix, given as

$$\mathbf{H} = \begin{bmatrix} \kappa^2 - \kappa_{01}^2 - h_{0101} & -h_{0102} & -h_{0103} & \cdots & -h_{01MN} \\ -h_{0201} & \kappa^2 - \kappa_{02}^2 - h_{0202} & -h_{0203} & \cdots & -h_{02MN} \\ -h_{0301} & -h_{0302} & \kappa^2 - \kappa_{03}^2 - h_{0303} & \cdots & -h_{03MN} \\ \vdots & \vdots & \vdots & & \vdots \\ -h_{MN01} & -h_{MN02} & -h_{MN03} & \cdots & \kappa^2 - \kappa_{MN}^2 - h_{MNMN} \end{bmatrix},$$

and $\mathbf{C}$ is the vector representation of the coefficients C_{mn} having $(\frac{M}{2}+1)\times N$ elements, given by

$$\mathbf{C}^T = [C_{01}\cdots C_{0N}\ C_{21}\cdots C_{2N}\cdots C_{M1}\cdots C_{MN}]$$

The condition that there be nontrivial solutions $\mathbf{C}$ is that

$$det\ \mathbf{H} = \mathbf{0} \tag{49}$$

This results in a series of perturbed eigenvalues for κ^2. We therefore reduce the complicated boundary value problem to a perturbative eigenvalue problem (Bender and Orzag, 1978).

Borehole Stoneley Wave

Because of the effects of the fracture, the sub-modes $\{\phi_{mn}\}$ are perturbed, and their associated eigenvalues κ_{mn} are modified, as given by the solutions of Eq. (49). The eigenvalue corresponding to the perturbed borehole Stoneley mode is the lowest order one of all the eigenvalues determined by Eq. (49). We designate this lowest order

eigenvalue by κ_{ST}^2. When κ_{ST}^2 is found by solving Eq. (49), the borehole Stoneley wavenumber k_z is given by

$$k_z = \sqrt{k_0^2 - \kappa_{ST}^2} \quad , \tag{50}$$

and the Stoneley phase velocity c_{ST} and attenuation coefficient α_{ST} are obtained from the real and imaginary part of k_z as

$$\begin{aligned} c_{ST} &= \frac{\omega}{Re\{k_z\}} \\ \alpha_{ST} &= Im\{k_z\} \quad . \end{aligned} \tag{51}$$

The attenuation of the perturbed Stoneley mode results from the loss of wave energy into the fracture. To illustrate how the presence of the fracture affects the borehole Stoneley propagation, we express κ_{ST}^2 by a series expansion of the secular determinant in Eq. (49) (Morse and Feshbach, 1953).

$$\begin{aligned} \kappa_{ST}^2 &= \kappa_{01}^2 + h_{0101} + \sum_{\substack{p\neq 0 \\ q\neq 1}} \frac{h_{01pq}h_{pq01}}{\kappa_{ST}^2 - \kappa_{pq}^2 - h_{pqpq}} \\ &+ \sum_{\substack{p,r\neq 0;\ q,s\neq 1 \\ r\neq p;\ q\neq s}} \frac{h_{01pq}h_{pqrs}h_{rs01}}{(\kappa_{ST}^2 - \kappa_{pq}^2 - h_{pqpq})(\kappa_{ST}^2 - \kappa_{rs}^2 - h_{rsrs})} + \cdots \end{aligned} \tag{52}$$

Thus if the fracture does not exist (i.e., $h_{mpnq} = 0$), κ_{ST} is given by $\kappa_{01} = \frac{\bar{\gamma}_0}{R}$, where $\bar{\gamma}_0$ is the root of Eq. (36) for $m = 0$. In fact, for $m = 0$ Eq. (36) reduces to the borehole dispersion equation (Eq. 9), and $\bar{\gamma}_0$ corresponds to the radial fluid wave number f in Eqs. (10). This gives the unperturbed Stoneley wavenumber

$$k_z^{(0)} = \sqrt{k_0^2 - \kappa_{01}^2} = \frac{\omega}{c} \quad , \tag{53}$$

where c is the borehole Stoneley velocity determined by Eq. (9). In the presence of the fracture, κ_{ST}^2 is given by the perturbation series in Eq. (52), with κ_{01} as the zero-order solution. The perturbations are in ascending orders of h_{mpnq}. From Eq. (46), we have, approximately,

$$h_{mpnq} \propto \frac{\omega L}{\pi R^2} \quad .$$

Therefore, at low frequencies or small fracture apertures, h_{mpnq} is small and κ_{ST}^2 can be well approximated by taking only the zero and first order terms. Thus

$$k_z = \sqrt{\frac{\omega^2}{c^2} + \frac{2L(-ik_y + h_0)[I_0(fR)]^2}{\pi R^2\{[I_0(fR)]^2 - [I_1(fR)]^2\}}} \quad , \tag{54}$$

where we have utilized h_{0101} given by Eq.(46). With increasing frequency (or aperture), κ_{ST}^2 in Eq. (52) involves higher order perturbation terms. In this situation, we must

increase M and N in Eq. (48) to yield accurate results. Physically, this means that the effects of higher frequency or larger fracture aperture will involve a higher degree of azimuthal (characterized by M) and radial (characterized by N) fluid motions. For a given frequency range and fracture aperture, M and N can be practically determined by comparing the numerical result at M, N with that at $M+1$, $N+1$. When the two results are sufficiently close, we may then reckon that the perturbation series in Eq. (52) converges to its true value at M and N. Since κ_{ST}^2 is the lowest order eigenvalue, it converges to its limit more rapidly than any other eigenvalues as M and N increase (Bender and Orzag, 1978). Therefore, moderate values of M and N will be sufficient to yield accurate results.

NUMERICAL EXAMPLES

In this section, we present the results on the effects of a vertical borehole fracture on the Stoneley propagation. Cases of both a hard and a soft formation are investigated, and the behavior of these effects will be illustrated in both low and higher frequency ranges.

Hard Formation

We first investigate the effects of the fracture for a hard formation. Figure 3 shows the results for a radius $R = 10$ cm borehole with a $L = 1$ cm fracture in a low frequency range of [0,2] kHz. For the formation, the compressional and shear velocities are V_p =5 km/s and V_s =3 km/s, respectively. The density ρ =2.5 g/cm^3. For the fluid, the acoustic velocity V_f = 1.5 km/s and the density $\rho = 1$ g/cm^3. Figure 3a shows the velocity dispersion of the Stoneley wave in the fractured borehole, plotted against the velocity of an unfractured borehole having the same radius. A prominent feature in this figure is the drastic decrease of the perturbed Stoneley velocity as frequency approaches zero while the unperturbed Stoneley velocity remains relatively unchanged. As discussed previously, this behavior is associated with the "slow wave" behavior of the fracture fundamental mode at low frequencies (Ferrazzini and Aki, 1987; Tang and Cheng, 1988). That is, the decrease in fracture wave velocity creates a large pressure gradient between the borehole and the fracture fluid, which drives the bore fluid effectively into the fracture, resulting in the retardation of wave propagation in the borehole. Figure 3b shows the calculated Stoneley wave attenuation coefficient in the same frequency range. The attenuation drastically increases with frequency to reach a maximum at low frequencies, then decreases with increasing frequency. In fact, the behaviors of Stoneley dispersion and attenuation at very low frequencies are well predicted by the first order theory given by Eq. (54). For a check of the theory, we plot both results from the first order theory (Eq. 54) and from the complete perturbation

theory (Eq. 49) in Figure 3b. The latter theoretical result is calculated by setting $M = 16$ and $N = 5$ in Eq. (48). Corresponding to Eq. (53), this result involves the summation of $(\frac{M}{2} + 1) \times N = 45$ perturbation terms, and should be regarded as quite accurate. As expected, the first order theory does not differ from the complete theory in the low frequency range. As frequency increases, the two theories begin to show some discrepancy, the attenuation from the first order theory being slightly higher than that from the complete theory. At higher frequencies, this discrepancy will be non-negligible and we should rely on the complete theory to yield accurate theoretical results. Figure 4 shows the Stonely wave dispersion (a) and attenuation (b) in a higher frequency range ([0,20]kHz) calculated using the complete perturbation theory. The parameters for the numerical evaluation are the same as those of Figure 3. In Figure 4a, we plot the Stoneley dispersion curve of the fractured borehole against that of an unfractured borehole of the same radius. Drastically increasing from small values at low frequencies, the perturbed Stoneley velocity becomes slightly higher than the unperturbed velocity in the medium frequency range. This can be expected since the opening of the fracture reduces the guiding effects of the borehole and the Stoneley velocity tends to move towards the free space velocity of the fluid. At high frequencies, both velocities approach the Scholte wave velocity (i.e., Stoneley velocity along a planar fluid-solid interface). Figure 4b shows the Stoneley attenuation coefficient as the function of frequency. Starting from a maximum at very low frequencies (see Figure 3b), the attenuation monotonically decreases with increasing frequency. On the basis of Figures 3 and 4, we see that the overall effects of a vertical fracture on the borehole Stoneley waves are very similar to those of a permeable borehole with a porous formation (Schmitt et al., 1988). Both types of effects involve dynamic fluid flow at the borehole wall and are more important in the very low frequency range than at higher frequencies.

Soft Formation

In the case of a soft formation whose shear velocity is less than the acoustic velocity of the fluid, the Stoneley wave velocity in the borehole and the fundamental mode velocity in the fracture are considerably lower than those in the case of a hard formation (for the fracture wave velocity, see Tang and Cheng, 1988). These effects are reflected in the term h_{mnpq} in Eq. (46), which governs the perturbation by the fracture. The soft formation or the slower Stoneley velocity causes the wall compliance $h_0 R$ to be much larger than that of a hard formation, particularly at high frequencies (Figure 2). On the other hand, the slower fracture wave velocity makes k_y have a larger value, especially at low frequencies. This results in the increase in the dynamic pressure gradient at the fracture opening and produces stronger borehole-fracture interaction. It is therefore expected that, in the low frequency range, the effect of a given fracture in the soft formation case will be more prominent than that in the hard formation case.

Figure 5 shows the Stoneley wave dispersion (a) and attenuation (b) in a low frequency range of [0,2] kHz. The borehole radius and the fracture aperture are the same as those in Figure 3. The formation and fluid velocities are: $V_p = 3$ km/s, $V_s = 1.4$ km/s, and $V_f = 1.5$ km/s. The formation and fluid densities are 2.5 g/cm^3 and 1 g/cm^3, respectively. As seen from Figure 5a, the perturbed Stonely velocity exhibits a similar behavior as we have seen and have discussed in Figure 3a, except that the difference between the perturbed and the unperturbed velocities are more significant than that in Figure 3a between 0.5 kHz and 2 kHz. The attenuation shown in Figure 5b also has similar behavior as that shown in Figure 3b. But the former is higher than the latter, because of the reasons already discussed. In addition, one also notices that the attenuation given by the first order theory begins to significantly differ from the one by the complete perturbation theory at about 1 kHz, because of the increased wall compliance. Figure 6 shows the Stoneley dispersion (a) and attenuation (b) in the frequency range of [0,20] kHz. The borehole radius and fracture aperture as well as the formation and fluid parameters are the same as those of Figure 5. The Stoneley velocity of a fractured borehole is significantly higher than the velocity of an unfractured borehole in the lower frequency range of Figure 6a. As frequency increases, both velocities approach the Scholte wave velocity corresponding to a soft solid-fluid interface. In Figure 6b, the attenuation of the Stoneley wave has its maximum value at very low frequencies (see also Figure 5b), then it rapidly decreases with increasing frequency. Beyond 10 kHz, the attenuation becomes very small. In the hard formation case shown in Figure 4b, the Stoneley attenuation is still significant even at 20 kHz. The fact that the Stoneley attenuation due to a fracture is most significant at low frequencies allows it to be separated from the intrinsic attenuation of the formation and fluid. The latter attenuation is small or negligible in the low frequency range.

LABORATORY EXPERIMENTAL EXAMPLES

We have theoretically analyzed the Stoneley wave propagation in a borehole with a vertical fracture. It is desirable to test the validity of our analysis. For this purpose, we carried out ultrasonic modeling experiments to measure Stoneley propagation in laboratory fracture borehole models.

Experimental Procedure

In the ultrasonic laboratory experiment, one must ensure that the borehole diameter lies in the range of ultrasonic wavelengths, so that the guided wave effects are easily measurable. Thus to simulate an in-situ Stoneley wave of peak frequency 5 kHz in a 20 cm diameter borehole, we scale our model borehole diameter to the order of 1 cm for a laboratory Stoneley wave with peak frequency around 100 kHz. The vertical fracture is

simulated by a saw cut in the model, which crosses the borehole diametrically and has an aperture on the order of 1 mm. We use aluminum to simulate the hard formation and lucite soft formation. They are shaped into cylinders. The aluminum cylinder is 20 cm in diameter and 25 cm in height. The lucite one is 15 cm in diameter and 18 cm in height. We use water as the borehole fluid. The acoustic properties of the three media are given in Table 1.

A diagram of the experimental setup is shown in Figure 7. An acoustic transducer is mounted at the bottom of the borehole model. The signal receiver is a small transducer located some distance above the source. During the experiment, the assembly designed in Figure 7 is submerged in a water tank. When the received waveform is digitized at a 0.4 μs sampling rate at a receiver position, the receiver is automatically moved to the next receiver position at a 1.8 mm step by a step motor controller. With about 50 receiver positions, a waveform array is obtained. We then apply the refined Prony's method (Ellefsen, 1988) to process the array data. Assuming the homogeneity of the formation and fluid along the array, this method of array processing involves changing the data from the time domain to frequency domain by applying a fast Fourier transform to each trace and then estimating the amplitude and phase for a propagating wave mode at every frequency using the method of least squares. The decay of amplitude along the array gives attenuation while the phase yields the phase velocity of the wave mode. Since we desire to measure the Stoneley wave attenuation and dispersion along the fractured borehole, this array processing technique is ideal for our purpose. For the velocity estimate, this technique yields accurate results, even when wave amplitude is small. For the attenuation estimate, one obtains reasonably accurate results when the signal-to-noise ratio of the wave is high. But the quality of the results will be degraded when this ratio is low.

Experimental Results

We first present the results of the hard formation fracture model experiment. Figure 8 shows the waveform array data for the aluminum model. The borehole radius R=1 cm and the fracture aperture L=1.1 mm. The Stoneley wave appears to be the dominant phase in this figure. It moves across the array at almost no noticeable dispersion. However, one can notice the decay of wave amplitude as source-receiver distance increases, particularly in the low frequency portion of the waves. This indicates that the Stoneley wave gradually loses its energy into the fracture in the propagation. The array data shown in Figure 8 are then processed using Prony's method. Figure 9 shows the estimated wave amplitude spectrum (a), attenuation coefficient (b), and the phase velocity (c) for the Stoneley wave. The attenuation and velocity are plotted versus the theoretical predictions calculated by solving Eq. (49) and using the parameters in Table 1. As shown in Figure 9b, in a broad frequency range of [0,400] kHz, both the predicted and measured attenuations decrease with increasing frequency. From 70 kHz

to 250 kHz in which the wave has most of its energy (see Figure 9a), the agreement is fairly good, although the measured values are a little higher than those of the theory towards the low frequency range. The theoretical and experimental velocity dispersions shown in Figure 11c show very good agreement throughout the frequency range. In particular, the decrease of velocity at very low frequencies — a characteristic of the effect of fracture as predicted by the theory — is detected by the experiment. Only in this very low frequency range does the perturbed Stoneley velocity have noticeable difference from the unperturbed (i.e., the intact borehole) Stoneley velocity in this particular case.

Next we show the results of the soft formation fracture model experiment. Figure 10 shows the waveform array data for the lucite model in which the borehole radius is 0.53 mm and the fracture aperture is 1.4 mm. The full waveform consists of a leaky-P (P) wave, a water wave (W), and a Stoneley wave (ST), as indicated in this figure. The leaky-P and water waves are typical of a soft formation (Chen, 1988) but they are of little interest at present. The Stoneley wave moves out approximately at a velocity of 1070 m/s, nearly the same as the Stoneley velocity without the effect of fracture. However, as one can notice from the figure, the Stoneley wave amplitude rapidly attenuates as the wave moves across the array. The array data shown in Figure 10 are then processed using Prony's method. Figure 11 shows the estimated wave amplitude spectrum (a), attenuation coefficient (b), and velocity dispersion (c). The theoretical predictions for the attenuation (b) and dispersion (c) are also plotted. Considering the fact that lucite is an attenuative medium, we calculated the intrinsic attenuation for the Stoneley wave using the theory of partition coefficient developed by Cheng et al. (1982). In this calculation, we neglected the presence of the fracture and used a shear quality factor $Q_s = 40$ for the lucite. As shown in Figure 11b, the intrinsic attenuation is linearly superimposed on the fracture attenuation (solid curve) to give the total attenuation (dashed curve). As expected, the total attenuation does not differ significantly from the fracture attenuation in the lower frequency range. As seen from the same figure, in the frequency range of [60,180] kHz in which the wave amplitude is the most significant, the measured attenuation shows little scatter and falls between the fracture attenuation and total attenuation curves. The agreement of the experiment with the theory is fairly good. The velocity estimate is shown in Figure 11c. The measured velocities are in very good agreement with the theory. Particularly, in the range of [60,180] kHz, the experimental results closely follow the theoretical velocity curve for a fractured borehole (solid curve), which is slightly higher than the velocity corresponding to an unfractured borehole with a soft (lucite) formation (dashed curve). At low frequencies, the measured velocities show the tendency to decrease with decreasing frequency, as predicted by the theory, although this tendency appears to occur at slightly higher frequencies.

CONCLUSIONS

We have presented a quantitative analysis of the Stoneley wave propagation in a fluid-filled borehole with a vertical fracture. This analysis is based on a boundary condition perturbation technique developed for the borehole situation, in which the change in the boundary condition due to the fracture is treated as the perturbation to the fluid-solid boundary condition at the borehole wall. To find this change in the boundary condition, we studied the fracture fluid motion excited by the borehole propagation. The boundary condition at the fracture opening can thus be specified by the interaction between the borehole wave and the fracture fundamental wave. The boundary condition perturbation technique reduces the complicated boundary value problem to a perturbative eigenvalue problem. The Stoneley wavenumber is obtained from the lowest order perturbed eigenvalue, giving the attenuation and velocity of the Stoneley wave as a function of frequency. Whatever the formation, hard or soft, significant Stoneley wave attenuation is produced because of the dynamic fluid flow occurring at the fracture opening. The attenuation is more significant at low frequencies than at higher frequencies. In the presence of intrinsic attenuation that is small at low frequencies, this behavior allows one to separate the two effects. The effects of a fracture on the Stoneley velocity are generally not very significant at higher frequencies. But they drastically reduce the Stoneley velocity at very low frequencies because of the increased borehole-fracture interaction. The theoretical predictions were found to agree well with laboratory experimental results for both hard and soft formation situations. Specifically, the decrease of Stoneley velocity at very low frequencies was observed by the experiment and the measured Stoneley attenuation was close to the theoretical values in the frequency range where the wave amplitude was high. The theoretical results of this study provide the quantitative relationship between Stoneley propagation and the character of a vertical fracture in connection with acoustic properties of the formation and fluid. The boundary condition perturbation technique developed in this study can be modified to study the effects of a vertical fracture on the propagation of other wave modes that exist in a borehole environment, such as pseudo-Rayleigh mode, leaky-P mode, and flexural wave mode.

ACKNOWLEDGEMENTS

We thank Karl J. Ellefsen for providing his program for the array data processing. This research was supported by the Full Waveform Acoustic Logging Consortium at M.I.T. and by Department of Energy grant No. DE-FG02-86ER13636.

REFERENCES

Abramowitz, M., and I.A. Stegun, *Handbook of Mathematical Functions*, New York, Dover Publications, Inc., 1970)

Bender, C.M., and S.A. Orzag, *Advanced Mathematical Methods for Scientists and Engineers*, New York, McGraw-Hill Book Company, 1978.

Biot, M.A., Propagation of elastic waves in a cylindrical bore containing a fluid; *J. Appl. Phys., 23*, 977–1005, 1952.

Chen, S.T., Shear-wave logging with dipole sources; *Geophysics, 53*, 659–667 1988.

Cheng, C.H., and M.N. Toksöz, Elastic wave propagation in a fluid-filled borehole and synthetic acoustic logs; *Geophysics, 46*, 1042–1053, 1981.

Cheng, C.H., M.N. Toksöz, and M.E. Willis, Determination of in situ attenuation from full waveform acoustic logs; *J. Geophys. Res., 87*, 5477–5484, 1982.

Doak, P.E., and P.G. Vaidya, Attenuation of plane wave and higher order mode sound propagation in lined ducts; *J. Sound Vib., 12*, 201–224, 1970.

Ferrazzini, V., and K. Aki, Slow waves trapped in a fluid-filled infinite crack: implication for volcanic tremor; *J. Geophys. Res., 92*, 9215–9223, 1987.

Ellefsen, K.J., Cheng, C.H., and Duckworth, G.L., Estimating phase velocity and attenuation of guided waves in acoustic logging data; *Expd. Abst., Soc. Expl. Geophys., 57th Ann. Int. Mtg. and Exposition*, New Orleans, LA, 1987.

Morse, P.M., and H. Feshbach, *Methods of Theoretical Physics*, New York, McGraw-Hill Book Company, 1953.

Paillet, F.L., and C.H. Cheng, A numerical investigation of head waves and leaky modes in fluid-filled boreholes; *Geophysics, 51*, 1438–1449, 1986.

Paillet, F.L., and J.E. White, Acoustic modes of propagation in the borehole and their relationship to rock properties; *Geophysics, 47*, 1215–1228, 1982.

Pilant, W.L., *Elastic Waves in the Earth*, Elsevier, (1979).

Schmitt, D.P., M. Bouchon, and G. Bonnet, Full-waveform acoustic logs in radially semiinfinite saturated porous media; *Geophysics, 53*, 807–823, 1988.

Tang, X.M., and C.H. Cheng, A dynamic model for fluid flow in open borehole fractures; *J. Geophy. Res.*, in press, 1989.

Tang, X.M., and C.H. Cheng, Wave propagation in a fluid-filled fracture–an experi-

mental study; *Geophy. Res. Lett., 15*, 1463–1466, 1988.

Watson, G.N., *A Treatise on the Theory of Bessel Functions*, London, Cambridge University Press, 1941.

Medium	ρ (g/cm^3)	V_p (m/sec)	V_s (m/sec)
Aluminum	2.7	6410	3180
Lucite	1.2	2740	1330
Water	1.0	1480	0

Table I: Density ρ, compressional velocity V_p, and shear velocity V_s of the fluid and solid used in the measurement.

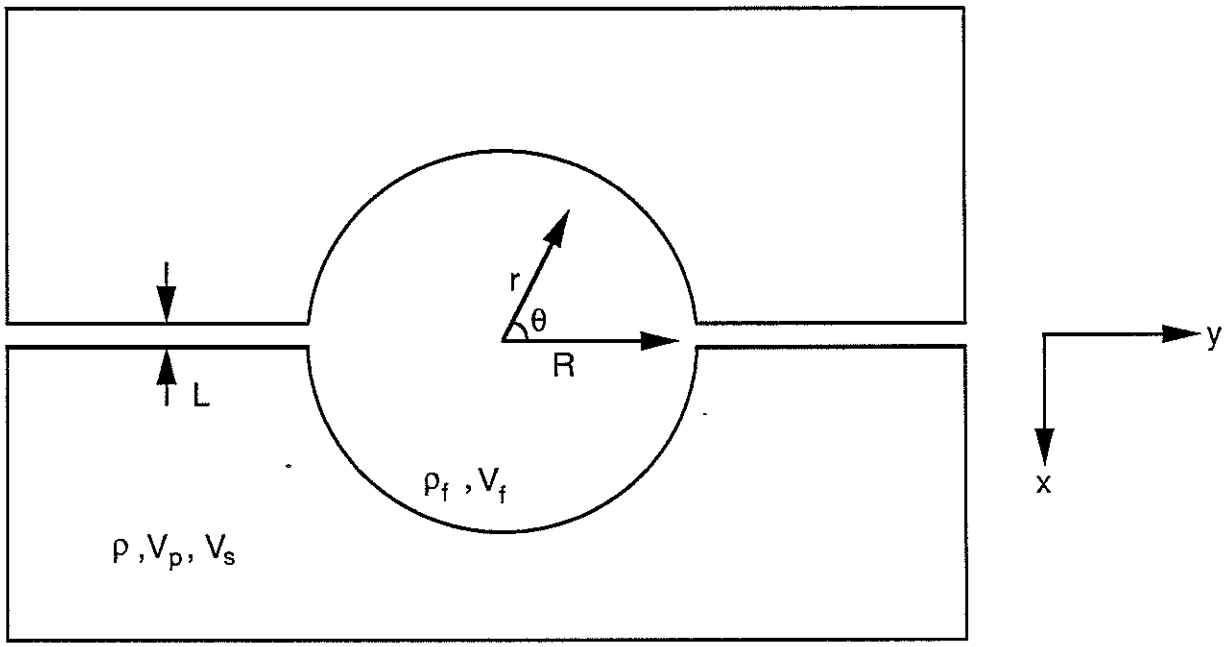

Figure 1: A cross-section of the borehole and fracture systems and their corresponding coordinates (r, θ, z) and (x, y, z). The z axes of the two systems are respectively at $r = 0$ and $x = y = 0$ and are pointing outwards from the figure.

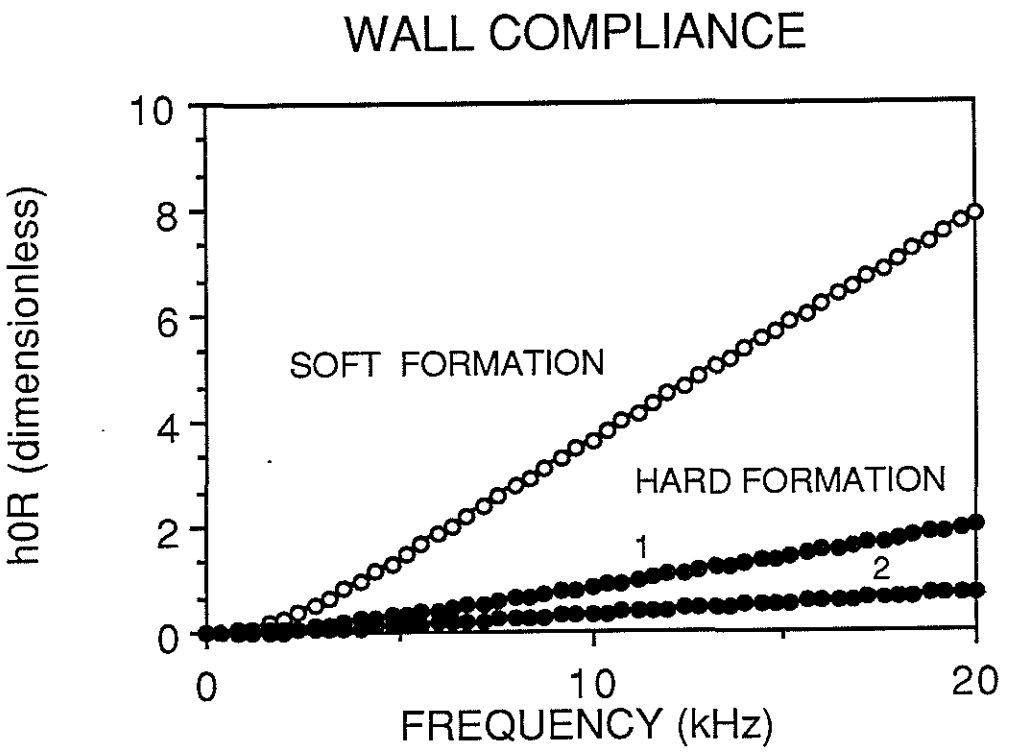

Figure 2: Wall compliance $h_0 R$ of hard (solid circles) and soft (open circles) formations versus frequency. The parameters are: $V_p = 3$ km/s and $V_s = 1.2$ km/s for the soft formation; $V_p = 5$ km/s and $V_s = 3$ km/s for the hard formation (1) and $V_p = 4$ km/s and $V_s = 2$ km/s for the hard formation (2). In all cases the formation density $\rho = 2.5\ g/cm^3$, the borehole has a radius of $R = 10$ cm and is filled with a fluid of $V_f = 1.5$ km/s and $\rho_f = 1\ g/cm^3$. Note that the compliance of a soft wall is much greater than those of hard walls.

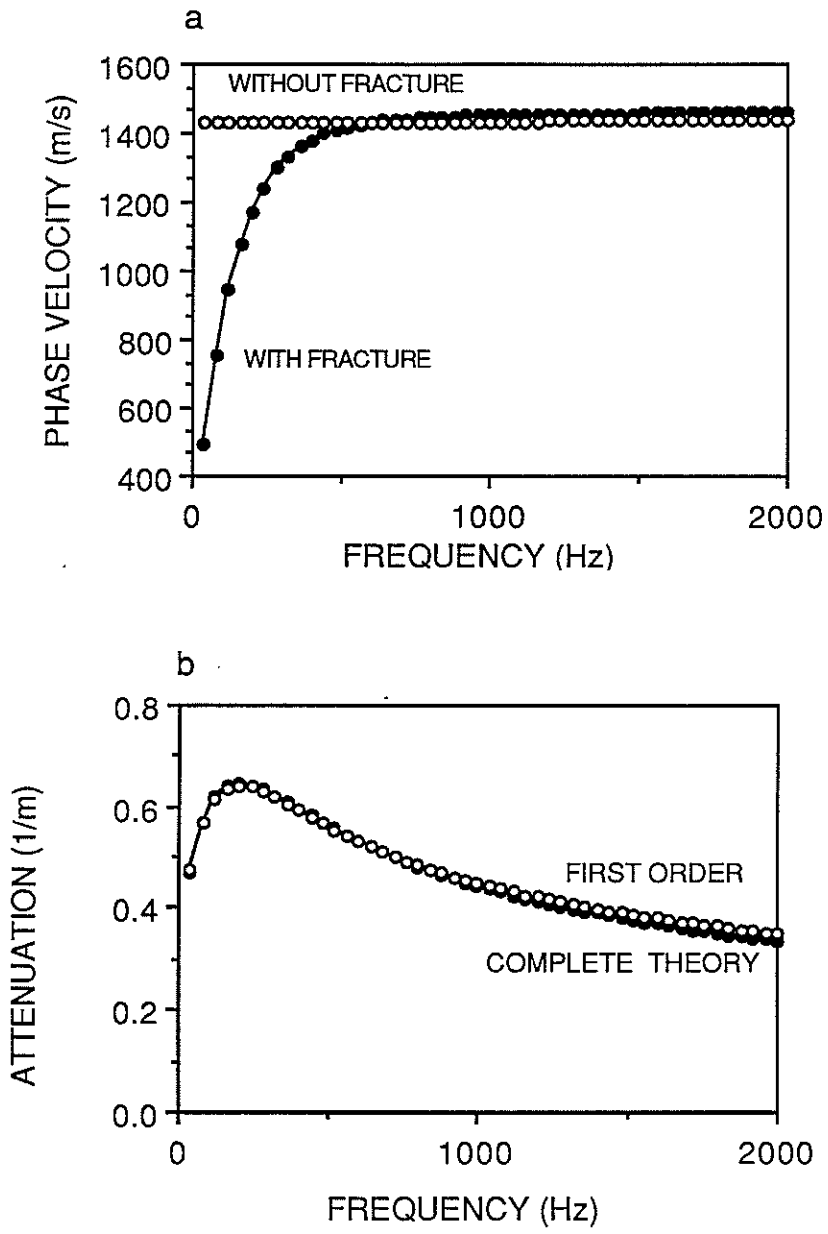

Figure 3: Stoneley wave dispersion (a) and attenuation (b) in the low frequency range for the hard formation case. As indicated in (a), the Stoneley velocity of a fractured borehole drastically decreases at very low frequencies. In (b) the Stoneley attenuations from the first order theory and from the complete perturbation theory are plotted. The two results are identical at low frequencies and begin to differ as frequency increases.

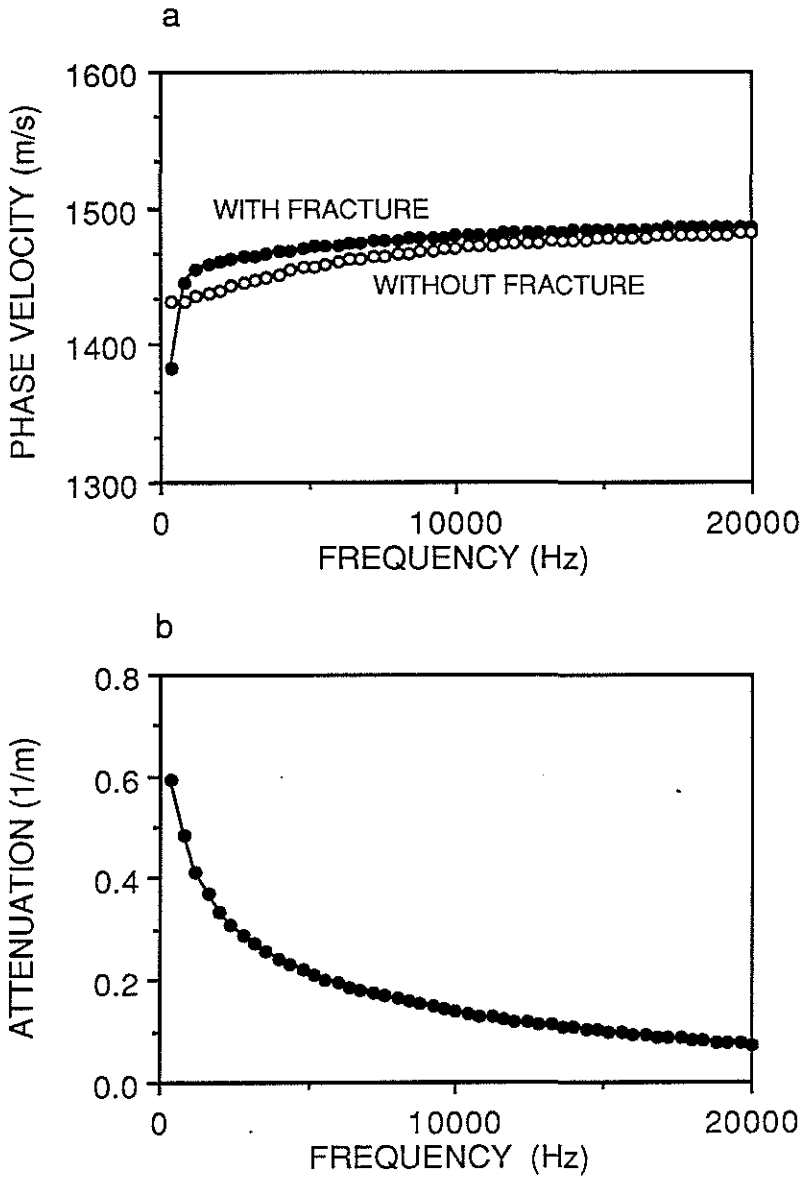

Figure 4: Stoneley dispersion (a) and attenuation (b) of Figure 3 in a higher frequency range. In (a) the perturbed velocity drastically increases to become slightly higher than the unperturbed velocity in the lower frequency range. Both velocities approach Scholte velocity as frequency increases. In (b) the Stoneley attenuation is the most significant at low frequencies and decreases as frequency increases.

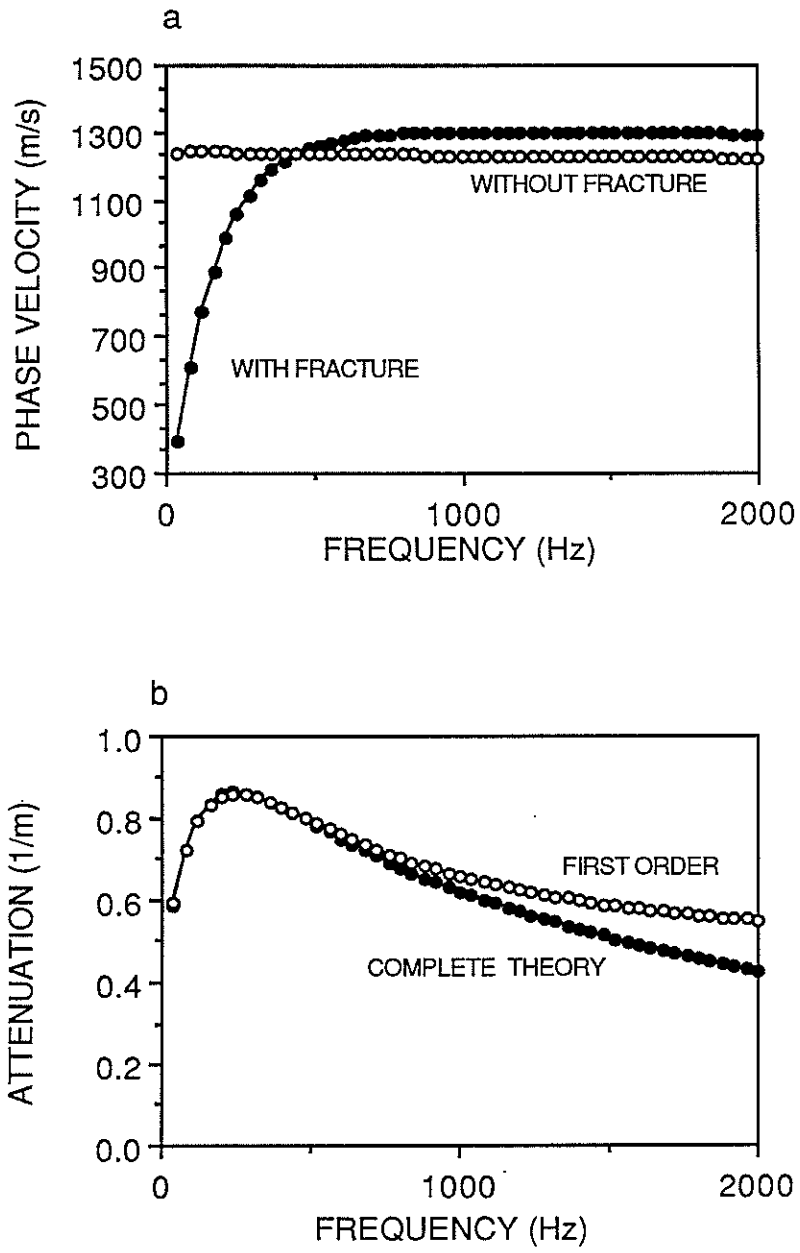

Figure 5: Stoneley dispersion (a) and attenuation (b) in the low frequency range for the soft formation case. In (a) the perturbed velocity exhibits the same behavior as in Figure 3a. In (b) the attenuation from the first order theory begins to diverge from that from the complete theory even in the low frequency range, because of the effects of the soft wall.

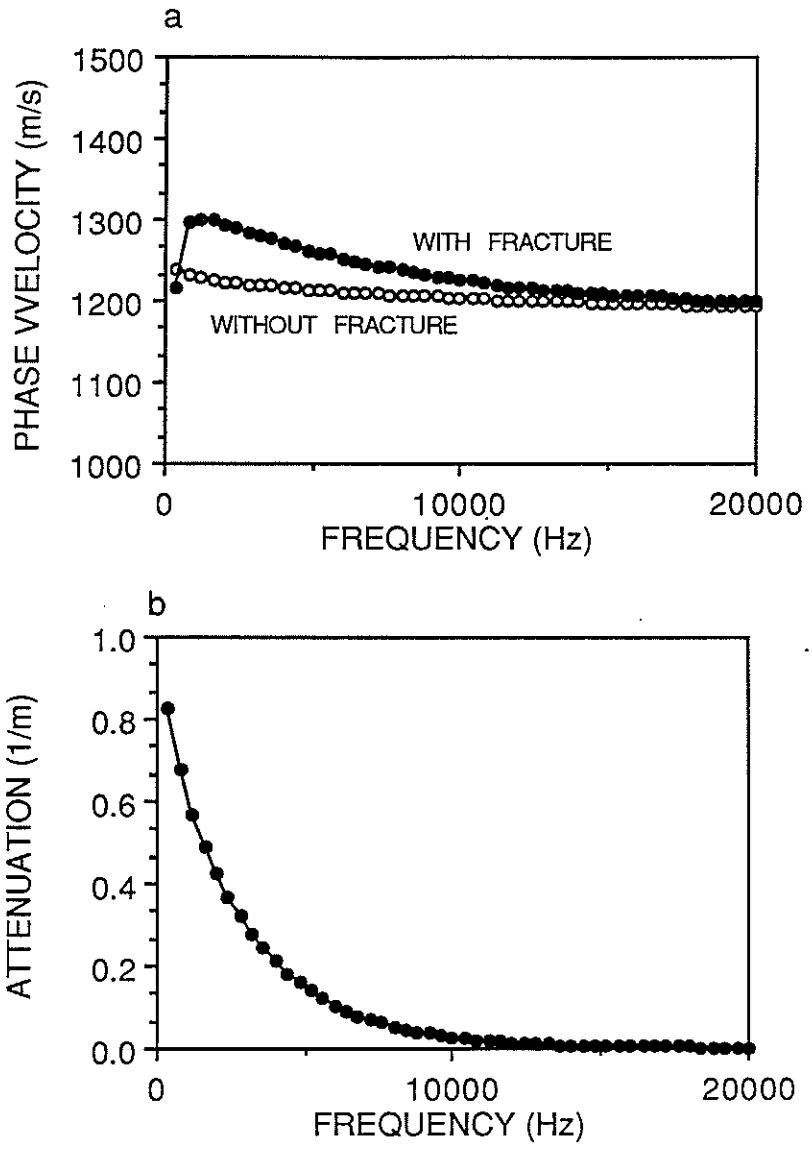

Figure 6: Stoneley dispersion (a) and attenuation (b) of Figure 5 in a higher frequency range. As shown in (a), the perturbed and the unperturbed velocities differ more significantly than what is shown in Figure 4b in the lower frequency range. Both velocities approach Scholte velocity along a soft solid-fluid interface as frequency increases. In (b) the attenuation is the most significant at low frequencies and rapidly decreases with increasing frequency.

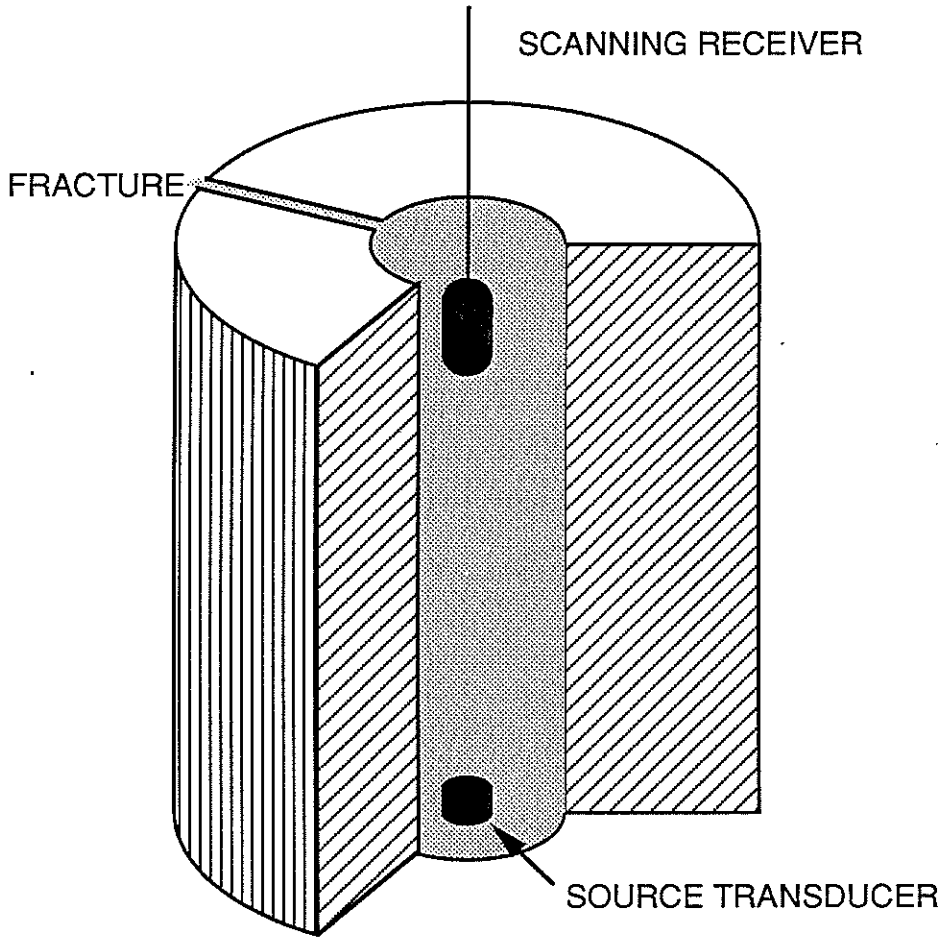

Figure 7: Experimental setup for measuring wave propagation in a fluid-filled borehole with a vertical fracture. The fracture is simulated by a saw-cut in the model. A transducer source is mounted at the bottom of the model while a receiver is placed into the borehole to measure the waves.

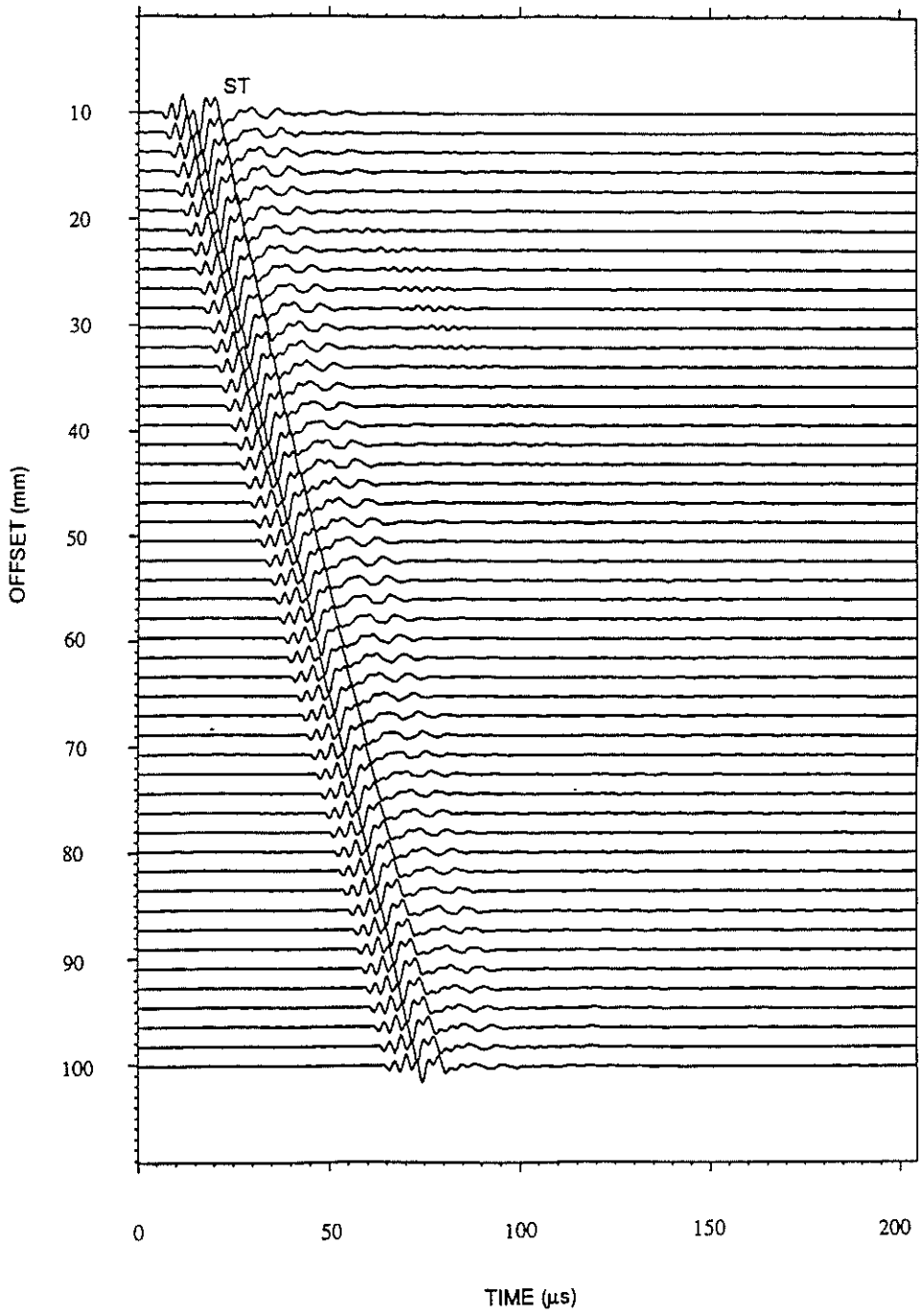

Figure 8: Experimental waveform array data received in the aluminum model at varying source-receiver distances. Note that the wave amplitude, particularly that of the lower frequency waves, gradually decreases as the source-receiver distance increases.

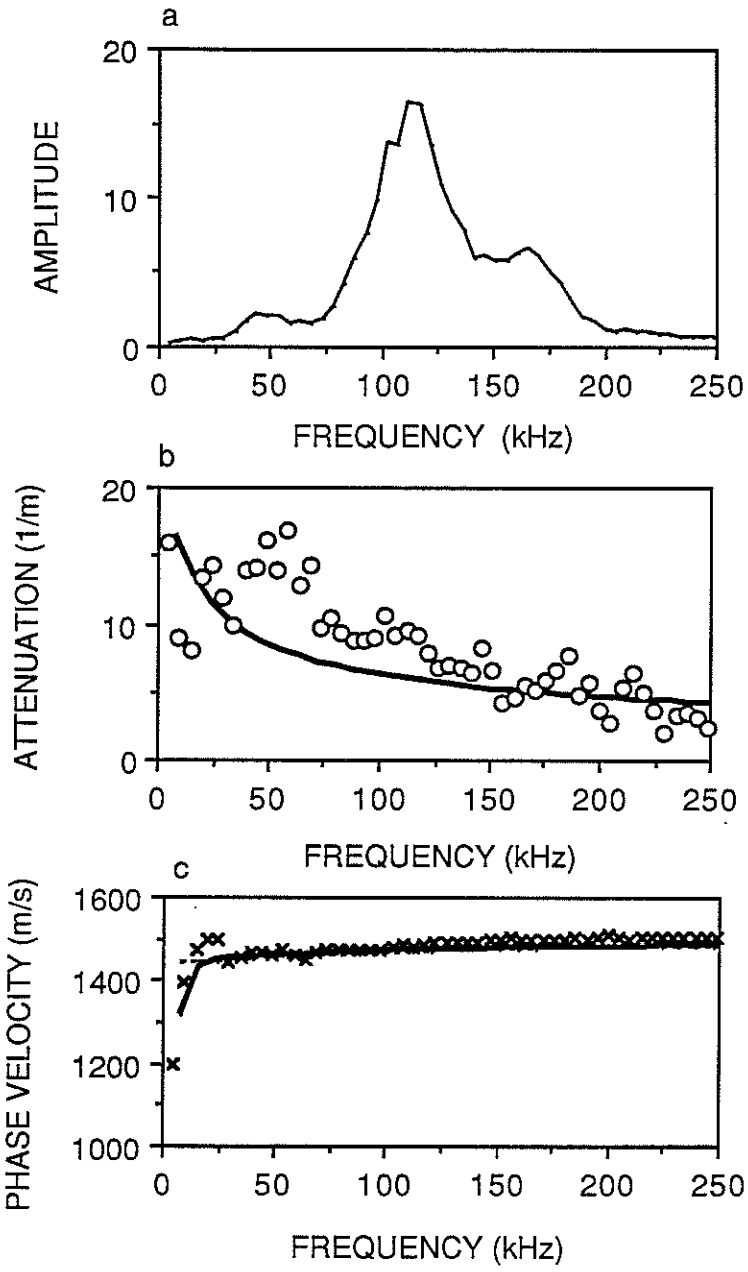

Figure 9: Experimental results versus theoretical predictions for the hard formation (aluminum) model. (a) Wave amplitude spectrum. (b) Measured Stoneley attenuation (open circles) and the theoretical attenuation (solid curve). (c) Measured Stoneley velocity (crosses) versus theory (solid curve). Note that in (c), at very low frequencies the experimental velocity decreases with decreasing frequency, as predicted by the theory.

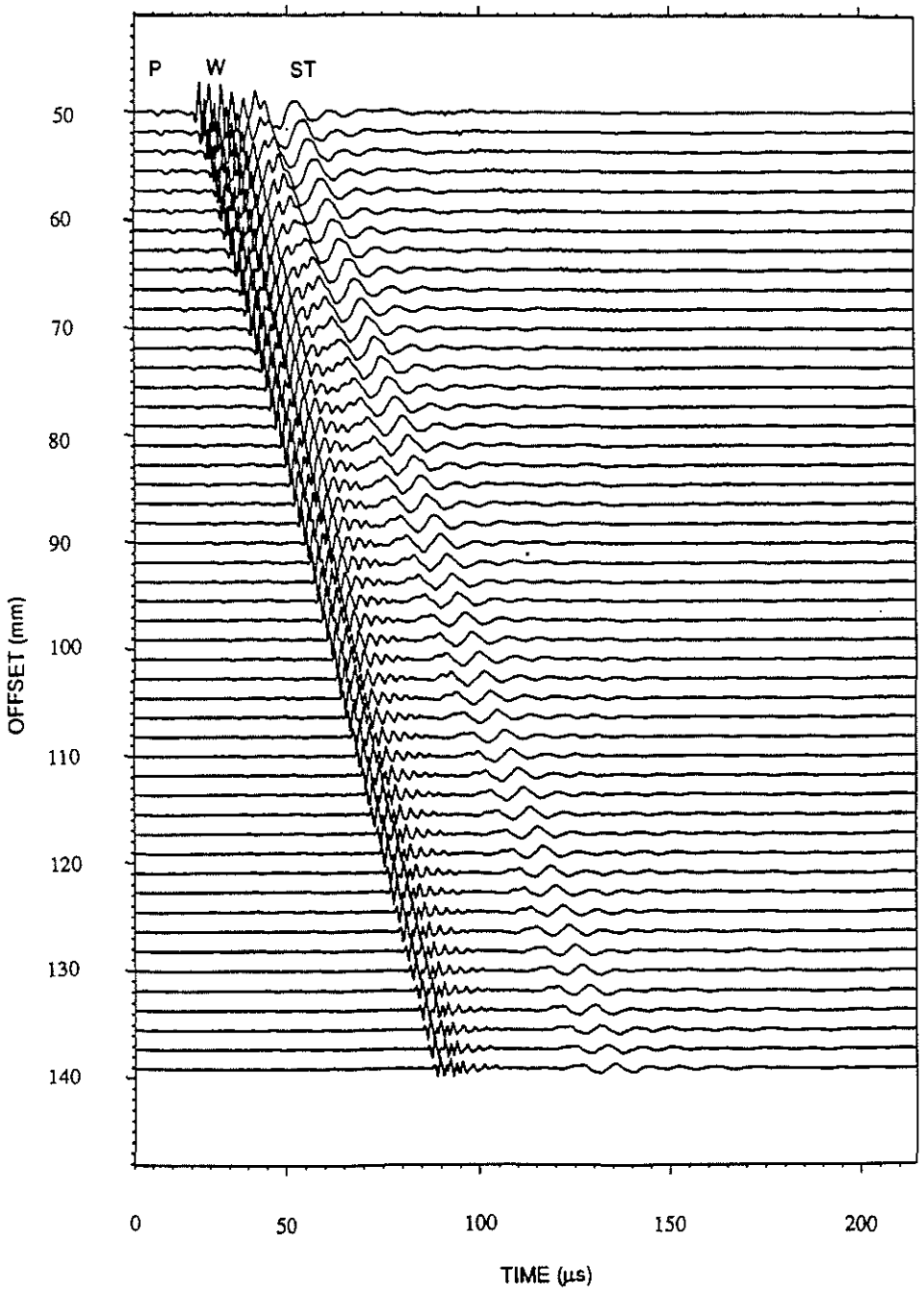

Figure 10: Waveform array data received in the lucite model. The labels are: P: leaky-P waves, W: "water" waves, and ST: Stoneley waves. Note that the Stoneley wave rapidly attenuates with increasing source-receiver distance.

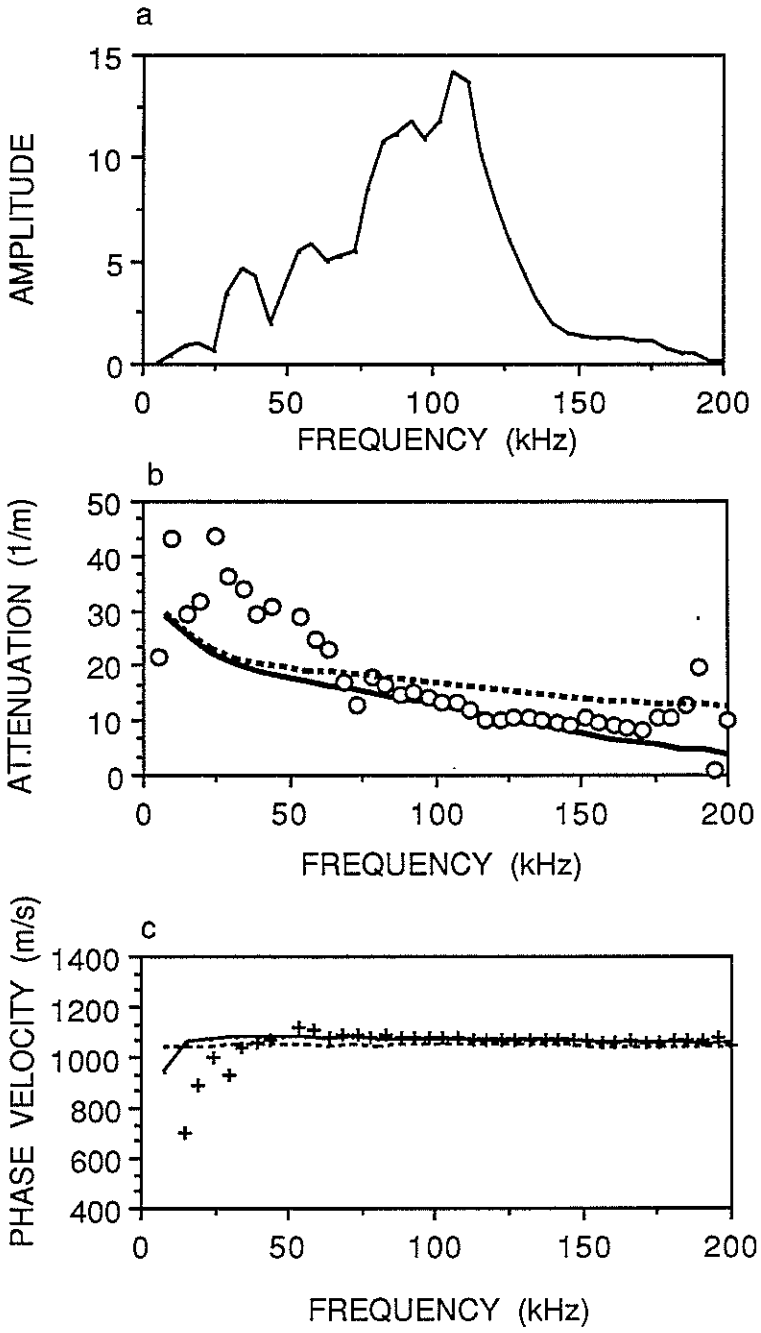

Figure 11: Experimental results versus theory for the soft formation (lucite) model. (a) Wave amplitude spectrum. (b) Measured Stoneley attenuation (open circles) and the theoretical attenuation (solid curve). (c) Measured Stoneley velocity (crosses) versus theory (solid curve). The Stoneley velocity of an unfractured borehole (dashed curve) is also plotted.